

Asteroseismic inference of the near-core magnetic field strength in the main sequence B star HD 43317

Daniel Lecoanet^{1,2,3*}, Dominic M. Bowman^{4,3}, Timothy Van Reeth^{4,3}

¹Department of Engineering Sciences and Applied Mathematics, Northwestern University, Evanston IL 60208, USA

²CIERA, Northwestern University, Evanston IL 60201, USA

³Kavli Institute for Theoretical Physics, University of California, Santa Barbara, CA 93106, USA

⁴Institute of Astronomy, KU Leuven, Celestijnenlaan 200D, B-3001 Leuven, Belgium

Accepted XXX. Received YYY; in original form ZZZ

ABSTRACT

About 10 per cent of intermediate- and high-mass dwarf stars are observed to host a strong large-scale magnetic field at their surface, which is thought to be of fossil field origin. However, there are few inferences as to the magnetic field strength and geometry within the deep interiors of stars. Considering that massive stars harbour a convective core whilst on the main sequence, asteroseismology of gravity (g) modes is able to provide constraints on their core masses, yet it has so far not been used to probe the strength of their interior magnetic fields. Here we use asteroseismology to constrain an upper limit for the magnetic field strength in the near-core region of the pulsating and magnetic B star HD 43317, based on the expected interaction of a magnetic field and its g modes. We find a magnetic field strength of order 5×10^5 G is sufficient to suppress high-radial order g modes and reproduce the observed frequency spectrum of HD 43317, which contains only high-frequency g modes. This result is the first inference of the magnetic field strength inside a main-sequence star.

Key words: asteroseismology – stars: magnetic field – stars: oscillations – stars: individual: HD 43317

1 INTRODUCTION

Magnetic fields are ubiquitous in astrophysics. However, observational constraints of internal magnetic fields of stars are limited. Large-scale magnetic fields have been detected at the surfaces of approximately 10% of massive dwarf stars (Power 2007; Shultz et al. 2012, 2018; Wade et al. 2014; Grunhut et al. 2017), typically from high-resolution spectropolarimetry (Wade et al. 2016). Most large-scale magnetic fields in massive stars have a predominantly dipolar geometry, which often is inclined to the rotation axis. The strengths of these fields are typically between 100 G and a few tens of kG. These large-scale magnetic fields likely extend deep within the radiative envelopes of massive stars, and are thought to be created during star formation (Mestel 1999; Neiner et al. 2015), but also form during binary mergers (Schneider et al. 2019). Irrespective of their origin, magnetic fields have a large impact on stellar structure and evolution (Maeder & Meynet 2005; Keszthelyi et al. 2019).

Asteroseismology — the study of stellar structure from oscillations — is a valuable tool to ascertain the interior physics of stars across the Hertzsprung–Russell (HR) diagram (Aerts et al. 2010; Aerts 2021). Waves restored by buoyancy are known as Internal Gravity Waves (IGWs), and those that set up standing waves are known as gravity (g) modes, which are extremely sensitive to the Brunt–Väisälä frequency profile. This makes g modes excellent probes of the convective core masses of main-sequence massive stars (Miglio et al. 2008; Bowman 2020; Johnston 2021). Furthermore, since massive

stars are commonly moderate-to-rapid rotators, the strength of the Coriolis force can be quantified from its impact on g modes (Bouabid et al. 2013). The asteroseismic diagnostic to constrain the rotation and core mass of main-sequence stars is the g-mode period spacing pattern, which typically spans up to a few dozen consecutive high-radial order prograde dipole g modes in main-sequence stars. The ‘tilt’ and asymptotic period spacing value probe the rotation rate and convective core mass, respectively (Van Reeth et al. 2016; Pápics et al. 2017; Mombarg et al. 2019; Pedersen et al. 2021).

The strength and geometry of an interior magnetic field can leave an imprint on g modes. Prat et al. (2019, 2020); Van Beeck et al. (2020) have made theoretical predictions for frequency shifts due to a magnetic field in rotating main-sequence stars and predict them to be very small for high-frequency g modes in such stars. So far, there have been no direct constraints of an internal magnetic field strength in the deep interior of a main-sequence star. In this work, we use the pulsating and magnetic B star HD 43317 to make the first observational inference of an interior magnetic field strength in a main-sequence star using asteroseismology.

2 HD 43317: A UNIQUE MAGNETIC PULSATOR

HD 43317 is a B3.5 V star with a precisely measured rotation period of 0.897673(4) d and a large-scale dipolar surface magnetic field with strength $B_p = 1312 \pm 332$ G from dedicated spectropolarimetric observations (Briquet et al. 2013; Buysschaert et al. 2017). High resolution spectroscopy of HD 43317 revealed it to likely be a single

* daniel.lecoanet@northwestern.edu

star with solar metallicity, a projected surface rotational velocity of $v \sin i = 115 \pm 9 \text{ km s}^{-1}$, an effective temperature of $T_{\text{eff}} = 17350 \pm 750 \text{ K}$ and a surface gravity of $\log g = 4.0 \pm 0.1$ (Pápics et al. 2012). HD 43317 was observed by the CoRoT mission (Auvergne et al. 2009) which provided a 150.5-d light curve with an average cadence of 32 s. The light curve contained dozens of significant g-mode frequencies (Pápics et al. 2012; Buysschaert et al. 2018).

Buysschaert et al. (2018) extracted all the significant g-mode frequencies from the CoRoT light curve of HD 43317. After delimiting the parameter space in the HR diagram using the spectroscopic parameters, the authors performed forward asteroseismic modelling to ascertain a statistically best-fitting mass of $M = 5.8^{+0.1}_{-0.2} M_{\odot}$, core hydrogen content of $X_c = 0.54^{+0.01}_{-0.02}$, and a parameterisation of convective boundary mixing (CBM) of $f_{\text{CBM}} = 0.004^{+0.014}_{-0.002}$. Assumptions in their modelling strategy included: rigid rotation fixed at the measured surface rotation period (i.e. $\approx 0.62 \Omega_{\text{crit, Roche}}$); constant envelope mixing of $D_{\text{env}} = 10 \text{ cm}^2 \text{ s}^{-1}$; and a radiative temperature gradient within the CBM region. The best-fitting parameters were derived based on a large grid of non-rotating and non-magnetic MESA structure models (r8118; Paxton et al. 2011, 2013, 2015) and corresponding theoretical pulsation mode frequencies using the stellar oscillation code GYRE (v4.1; Townsend & Teitler 2013) after identifying probable mode geometries of the detected g-mode frequencies. The effect of rotation was included within the GYRE calculations using the Traditional Approximation for Rotation (TAR; Townsend & Teitler 2013). We refer the reader to Buysschaert et al. (2018) for full details.

HD 43317 is the only magnetic and rapidly rotating star pulsating in g modes that has been modelled using asteroseismology (Buysschaert et al. 2018). For (non-magnetic) pulsating stars in this mass range (i.e. SPB stars), much higher radial orders (i.e. $|n_{\text{pg}}| \gg 1$) are more commonly observed (Pedersen et al. 2021), making HD 43317 atypical given its distinct lack of high-radial order g modes.

In Fig. 1, we show the propagation diagram for the structure model determined by Buysschaert et al. (2018) to best reproduce the observed g-mode frequencies and inferred mode geometry identification. In this paper we primarily study this best-fitting structure model and determine an upper limit of the magnetic field strength in the near-core region that satisfies the constraint that HD 43317 only has high-frequency g modes. To test the robustness of our results, we also analyse an additional 19 models which satisfy the 2σ confidence intervals on mass, age and CBM (see Table 2 of Buysschaert et al. 2018). Although there are many free parameters that can be included when calculating a grid of structure models, we consider the asteroseismically calibrated models of Buysschaert et al. (2018) to be sufficient to test the hypothesis that the interior magnetic field is strong enough to suppress low-frequency g modes and explain why only high-frequency g modes are observed.

3 INTERACTION OF INTERNAL GRAVITY WAVES AND MAGNETIC FIELDS

The magnetic SPB star HD 43317 has only high-frequency g modes observed in its amplitude spectrum of the CoRoT light curve, with radial orders spanning $-15 \leq n_{\text{pg}} \leq -1$, which is atypical for SPB stars (Buysschaert et al. 2018). The lowest-frequency g mode is $f_g = 1.806 \text{ d}^{-1}$ in the corotating frame, which leads to the question of why lower frequency g modes are not observed. Non-adiabatic pulsation calculations of HD 43317 using GYRE (v6.0.1; Townsend & Teitler 2013; Townsend et al. 2018; Goldstein & Townsend 2020) suggest a wider range of g modes should be excited, with n_{pg} ranging

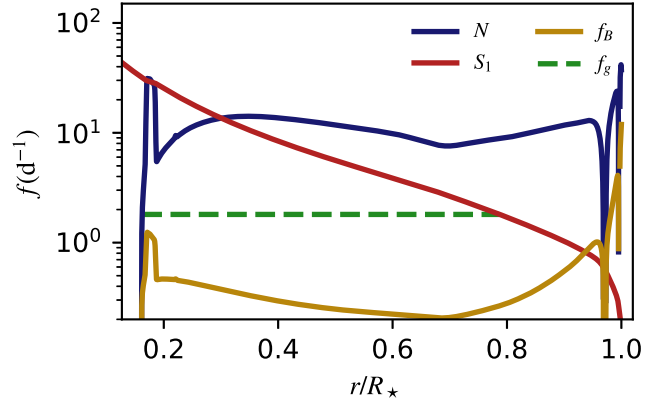


Figure 1. Propagation diagram for the magnetic SPB star HD43317 using the best-fitting asteroseismic model of Buysschaert et al. (2018). The green line shows the oscillation cavity of the lowest-frequency identified g mode with frequency $f_g = 0.692 \text{ d}^{-1}$ in the inertial frame. The yellow line is an estimate of the magnetic interaction frequency for $\ell = 1$, assuming the magnetic field is a dipole with strength $B_r = 4.68 \times 10^5 \text{ G}$ at $r = 0.18 R_*$ (eqn. 1).

from -39 ± 2 to -8 ± 1 for $(\ell, m) = (2, -1)$ and from -34 ± 3 to -8 ± 1 for $(\ell, m) = (1, -1)$. We propose that these low-frequency g modes are suppressed by a strong near-core magnetic field.

To understand the suppression of g modes, we turn our attention to propagating IGWs. If an IGW can reflect off an upper and lower region of a star and its frequency satisfies a quantization condition, it can set up a standing mode, i.e., a g mode. Fuller et al. (2015) and Lecoanet et al. (2017) found that IGWs can have strong interactions with magnetic fields which prevent them from reflecting off the inner part of the star. This can suppress the dipole oscillation modes in RGB stars (e.g., Stello et al. 2016). They found that (ignoring rotation) if an IGW of frequency f enters a region where

$$f \lesssim f_B = \frac{1}{2\pi} \sqrt{\frac{B_r}{\rho}} \frac{N\Lambda}{r}, \quad (1)$$

it can convert into a magnetic wave, preventing the formation of a standing g mode. Here B_r is the radial magnetic field, ρ is the density, $\Lambda = \sqrt{\ell(\ell+1)}$ with ℓ the spherical harmonic degree of the IGW, and r is the local radius. This relation was used to estimate a magnetic field of $\sim 10^7 \text{ G}$ in the RGB star KIC 8561221 (García et al. 2014; Fuller et al. 2015). Assuming (as a rough approximation) the interior magnetic field of HD 43317 varies as $1/r^3$ like a dipole, Fig. 1 shows that f_B is greatest in the near-core region at $r \approx 0.18 R_*$, if we only consider the oscillation cavities of the identified observed g modes of HD 43317 which have frequencies above the green line. This indicates that the strongest interaction between IGWs and a dipolar magnetic field would occur in the near-core region where N is large due to the chemical composition gradient. In this region $f_B \sim 1 \text{ d}^{-1}$, indicating that magnetic and rotational effects are similar in strength. A similar calculation by Cantiello et al. (2016), also found magnetic fields of 10^5 G can suppress modes with $f \lesssim 0.86 \text{ d}^{-1}$.

To refine this heuristic estimate, we calculate the linear waves of a rotating, magnetised star using the WKBJ approximation. We assume the background magnetic field is predominately dipolar, and take $B_r(r, \theta) = B_r(r) \cos(\theta)$. We assume all wave variables can be written as, e.g.,

$$U_r(r, \theta, \phi, t) = u_r(r, \theta) \exp \left[i m \phi - i \omega t + i \epsilon^{-1} \int \psi(r) dr \right], \quad (2)$$

where m is the azimuthal wavenumber, $\omega = 2\pi f$ is the angular frequency, $u_r(r, \theta)$ is an amplitude, and ψ is the phase. The local radial wavenumber is $k_r = \epsilon^{-1} \psi'(r)$. The WKB approximation is an exponentially-accurate asymptotic expansion in the small parameter $\epsilon \sim f/N$. Assuming $N \sim B_r \sim O(\epsilon^{-1})$ and all other parameters are $O(1)$, the leading order oscillation equations are

$$N(r)^2 u_r + k_r p = 0, \quad (3)$$

$$-i\omega \mathbf{u}_h + 2\boldsymbol{\Omega} \times \mathbf{u}_h + r^{-1} \nabla_h p = iB_r(r) \cos(\theta) k_r \mathbf{b}_h, \quad (4)$$

$$r^{-1} \nabla_h \cdot \mathbf{u}_h + ik_r u_r = 0, \quad (5)$$

$$-i\omega \mathbf{b}_h - iB_r(r) \cos(\theta) k_r \mathbf{u}_h = -\eta k_r^2 \mathbf{b}_h. \quad (6)$$

Only the radial component of the magnetic field enters to leading order in ϵ .

The perturbations are given by the radial velocity u_r , horizontal velocity and magnetic field \mathbf{u}_h and \mathbf{b}_h , and pressure p . The rotation vector is $\boldsymbol{\Omega}$, ∇_h gives the angular components of the gradient, and η is the magnetic resistivity. For a given oscillation frequency ω , the calculation is an eigenvalue problem at each radius with eigenvalue k_r . We solve this eigenvalue problem in spherical geometry with the DEDALUS code (Vasil et al. 2019; Lecoanet et al. 2019; Burns et al. 2020). The scripts used to generate the data and plots in this paper can be found at <https://github.com/lecoanet/HD43317-B>.

4 RESULTS

In Fig. 2 we plot the radial wavenumber for different waves with $m = -1$ and $f = 0.872 \text{ d}^{-1}$ assuming a dipolar magnetic field with $B_r = 4.68 \times 10^5 \text{ G}$ at $r = 0.18R_\star$, and a magnetic resistivity $\eta = 0$. We use the frequency of the observed g mode with $\ell = 2$ and $n_{\text{pg}} = -15$; this is the lowest frequency $\ell = 2$ mode observed by Buysschaert et al. (2018) for HD 43317. The radial wavenumbers of the IGWs remain modest until they enter the chemical composition gradient region. At high wavenumbers, we find a continuum of resonant Alfvén waves (AWs). These AWs have critical latitudes, and those with wavenumbers in the lower part of the blue shaded region of Fig. 2 have critical latitudes near the poles. When the radial wavenumber of an IGW enters the blue shaded region, it turns into a resonant AW, and its energy is spread out amongst the continuum modes. When this occurs, the wave cannot return to the surface as an IGW; thus the wave cannot set up a g mode. The $\ell = 1$ and $\ell = 2$ IGWs with $f = 0.872 \text{ d}^{-1}$ and a magnetic field strength of $B_r = 4.68 \times 10^5 \text{ G}$ do not turn into AWs. Thus, they can reflect off the radiative-convective interface, return to the surface as IGWs, and set up g modes. Although the wavenumber of the $\ell = 2$ IGW just barely enters the AW region, the IGW is equatorially confined, which means it has exponentially weak overlap with the near-polar resonant AWs. Finally, we note that the radial wavenumber changes abruptly at the edge of the chemical composition region (vertical dashed line in Fig. 2). There may also be wave reflection off this point.

If the magnetic field strength is slightly higher, an IGW of the same frequency turns into an AW near the radiative-convective interface. We define the critical magnetic field B_{crit} to be the threshold radial magnetic field strength at $r = 0.18R_\star$, over which an IGW turns into an AW as it propagates into the star. This is a more precise version of the f_B heuristic argument of Eqn. 1. In Fig. 3 we plot B_{crit} for IGWs with frequencies which match theoretical mode frequencies calculated using GYRE. IGWs with frequencies of observed g modes are plotted with thick symbols, and IGWs with frequencies of unobserved g modes are plotted with thin symbols. The lowest frequency modes for each ℓ have the smallest B_{crit} . For the $(\ell, m) = (2, -1)$ mode with

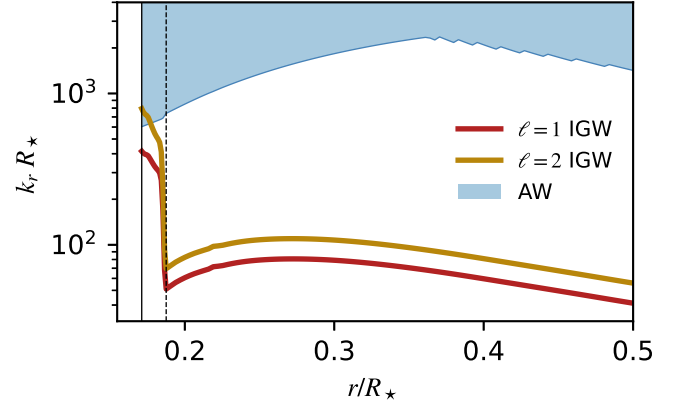


Figure 2. Radial wavenumber as a function of radius for $\ell = 1$ and $\ell = 2$ IGWs (red and yellow lines), and resonant Alfvén waves (AWs; shaded blue region), assuming $B_r = 4.68 \times 10^5 \text{ G}$ at $r = 0.18R_\star$. The waves have $m = -1$ and $f = 0.872 \text{ d}^{-1}$. The vertical solid and dashed lines are the radiative-convective boundary, and the boundary of the chemical composition gradient region. The IGWs do not interact with the AWs, so they can reflect off the radiative-convective interface and produce g modes.

frequency $f = 0.872 \text{ d}^{-1}$, we have $B_{\text{crit}} \approx 4.7 \times 10^5 \text{ G}$, whereas for the $(\ell, m) = (1, -1)$ mode with frequency $f = 0.692 \text{ d}^{-1}$, we have $B_{\text{crit}} \approx 6.1 \times 10^5 \text{ G}$. This means, e.g., a near-core magnetic field of $\approx 4.7 \times 10^5 \text{ G}$ would suppress all lower frequency $\ell = 2$, $m = -1$ modes. This gives a natural explanation for the lack of low-frequency g modes in HD 43317. The fact that the lowest frequency observed modes for each ℓ have similar B_{crit} supports this theory. In summary, the largest magnetic field consistent with the observed g modes has a strength of $B_r \approx 4.7 \times 10^5 \text{ G}$ at $r = 0.18R_\star$.

There are two unobserved $\ell = 1$ modes with $B_{\text{crit}} > B_r$, which would not be suppressed by this magnetic field. These modes might not be observed because: (i) The modes are not excited to observable amplitudes; or (ii) The magnetic field near the radiative-convective interface is not entirely dipolar, leading to a different ℓ -dependence of B_{crit} . In addition, Buysschaert et al. (2018) found three other oscillation modes which they could not identify with inertial-frame frequencies of $< 0.692 \text{ d}^{-1}$. Our analysis suggests these are $m = -2$ modes which have large frequencies in the corotating frame, and thus are not strongly affected by the magnetic field.

To demonstrate the interaction between IGWs and a dipolar magnetic field, we plot two inward and outward propagating waves in Fig. 4. On the left we plot $u_\phi(\phi = 0)$ for an IGW with $f = 0.872 \text{ d}^{-1}$ in the inertial frame, which corresponds to the frequency of the $n_{\text{pg}} = -15$ g mode, the lowest-frequency observed $\ell = 2$ mode. We plot the WKB solution described by Eqn. 2, where we take $t = 0$, and normalise $u_\phi(r, \theta)$ according to $\int |u_\phi|^2 \sin(\theta) d\theta = 1$. The next-to-leading-order equations could be used to derive an equation for the amplitude as a function of r . The inward propagating wave (top left) has $k_r > 0$, and is initialised with a phase of $\pi/2$ at $r = 0.5$. The outward propagating wave (bottom left) has $k_r < 0$, and matches the phase of the incoming wave at the radiative-convective interface. Although the wave has a small radial wavenumber in the chemical composition gradient region, it can reflect off the radiative-convective interface and set up a g mode.

On the right of Fig. 4, we plot u_ϕ in the same way for an IGW with $f = 0.840 \text{ d}^{-1}$, which corresponds to the frequency of the $n_{\text{pg}} = -16$ g mode, which is not observed. As this wave propagates

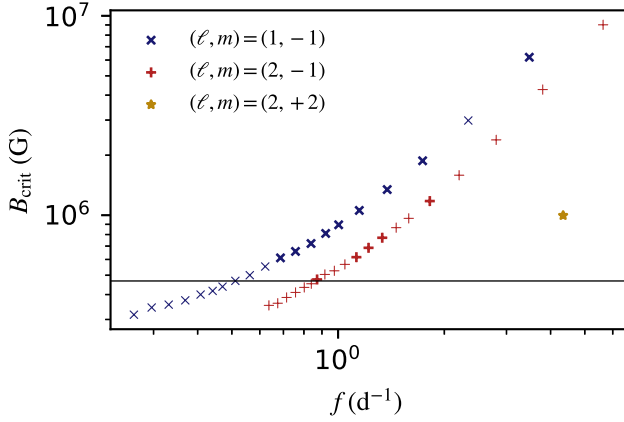


Figure 3. Critical magnetic field strength for different IGWs as a function of their frequency in the inertial frame. We study waves with the frequencies of the g modes of HD 43317. Frequencies corresponding to observed (unobserved) modes are plotted with thick (thin) symbols. We infer a magnetic field with strength $B_r \approx 4.7 \times 10^5$ G at $r = 0.18R_\star$ (horizontal line). A dipolar field of this strength would suppress g modes below the horizontal line, explaining the lack of low-frequency modes.

inwards (upper right plot), it exhibits similar behaviour to the higher-frequency mode as the left hand side of the figure. However, near the radiative-convective interface, it undergoes a strong interaction with the magnetic field, turning into a resonant AW. In the bottom right quadrant of Fig. 4, we show the structure of the resonant AW. We calculate the AW at a single radius near the radiative-convective interface, but plot it at a range of radii to illustrate its structure. To resolve the AW, we introduce a small magnetic resistivity of $\eta = 3 \times 10^{-10}$ into the problem. The AW has high radial wavenumber and a critical latitude near 45° . Because the resonant AWs form a continuum (Fig. 2), we expect the AW to interact with many other AWs and spread across many latitudes. This means no IGW returns to the surface at this frequency, so there is no g mode, in agreement with the observed properties of the star.

There is uncertainty in the stellar structure of HD 43317 as inferred from asteroseismology. Up to now, we have analysed the best-fitting structure model. To test the robustness of our inferred magnetic field strength, we calculate B_{crit} using the structure models from Buyschaert et al. (2018) which satisfy the 2σ confidence intervals on mass, age and CBM. In Fig. 5, we plot B_{crit} for the IGWs with the frequencies of the $(\ell, m) = (2, -1)$ modes with $n_{\text{pg}} = -16$ and $n_{\text{pg}} = -15$. Assuming the $n_{\text{pg}} = -16$ mode is not observed at the surface due to the presence of a dipolar magnetic field, the magnetic field strength must be between these two B_{crit} . To estimate this magnetic field strength, we plot the histogram of the mean of B_{crit} for these two modes. The average magnetic field strength across the 20 best-fitting models is $B_r = 456$ kG in the near core region, $r \approx 0.18R_\star$. The root-mean-square deviation from this mean across the twenty models is 6 kG. The inferred magnetic field strength is insensitive to the different models.

5 CONCLUSIONS

Magnetic massive stars are rare, and pulsating magnetic massive stars are rarer still. The pulsating, magnetic and rapidly rotating star HD 43317 provides a unique opportunity to infer the strength of the magnetic field in the near-core region based on the reported

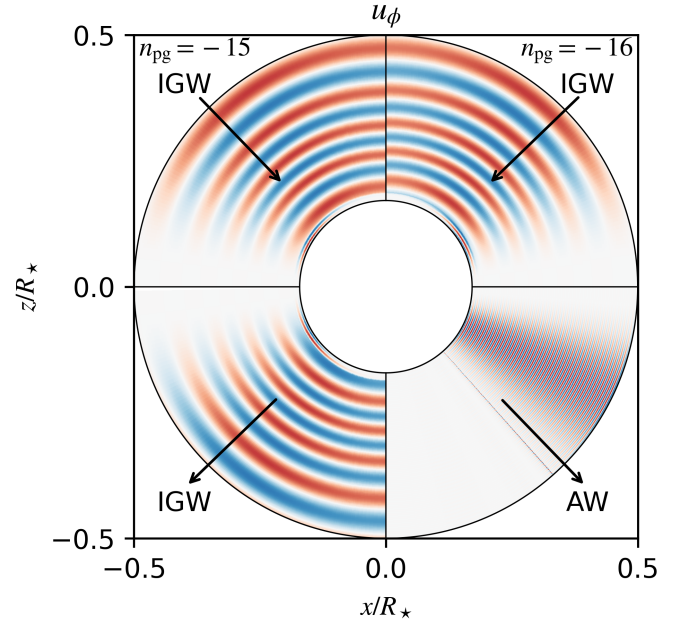


Figure 4. Azimuthal velocity structure for $m = -1$, $\ell = 2$ waves with frequencies $f = 0.872 \text{ d}^{-1}$ (left; $n_{\text{pg}} = -15$) and $f = 0.840 \text{ d}^{-1}$ (right; $n_{\text{pg}} = -16$) in the inertial frame, assuming a dipole magnetic field with $B_r = 4.68 \times 10^5$ G at $r = 0.18R_\star$. The top panels show the incoming waves, and bottom panels show outgoing waves. The lower frequency wave, corresponding to the unobserved $n_{\text{pg}} = -16$ mode, interacts strongly with the magnetic field when it enters into chemical composition gradient region, triggering a latitudinally-localised resonant AW. The AW is calculated only at a single radius near the radiative-convective interface, but is plotted over a range of radii to give a sense of its structure.

lack of observed low-frequency g modes (Buyschaert et al. 2018). To reproduce the lowest-frequency observed g mode based on the previous forward asteroseismic modelling, we find a critical magnetic field strength of approximately 5×10^5 G is needed in the near-core region for HD 43317. This inference is the first of its kind for a main-sequence star and serves as a valuable proof-of-concept for two reasons. First, pulsation modes can diagnose interior magnetic fields. Second, the interaction of waves with a strong internal magnetic field can explain why only certain radial order modes are visible at the surface of HD 43317.

What is the physical origin of this magnetic field? HD 43317 has a surface magnetic field of strength ≈ 1.3 kG. If the strength of the field scales as $\sim r^{-3}$ from the surface to the interior of the star, the field in the near-core region would be $B_r \sim 200$ kG, which is smaller than our inferred field strength by a factor of ≈ 2 . It is also possible that the near-core magnetic field is enhanced by a core convective dynamo. 3D simulations of B stars find magnetic field strengths of ≈ 200 kG (Augustson et al. 2016). However, Featherstone et al. (2009) found the presence of a fossil field can enhance the dynamo magnetic field up to ≈ 500 kG, as we find here. Our results support the conclusion that HD 43317’s near-core magnetic field is a stronger-than-normal core convective dynamo induced by a strong fossil field, which is observed at the star’s surface.

In the future, we anticipate that this methodology can be expanded and applied to potentially many more pulsating magnetic stars being discovered by the ongoing NASA TESS mission (Ricker et al. 2015). Thus, measuring near-core field magnetic field strengths sampling mass and age on the upper-main sequence is now within reach.

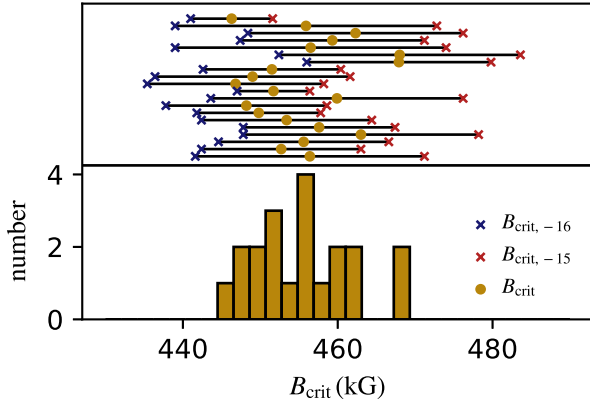


Figure 5. Top panel: Critical magnetic field strength for the 20 best fitting asteroseismic models. Blue (red) crosses show B_{crit} for IGWs with frequency of the $\ell = 2$, $n_{\text{pg}} = -16$ ($n_{\text{pg}} = -15$) modes. The yellow circles show their mean, as estimate of the stellar magnetic field. Bottom panel: Histogram of the estimated magnetic field strength. We infer $B_r = 456 \text{ kG}$ with an rms deviation across the 20 models of 6 kG.

ACKNOWLEDGEMENTS

The authors thank Jim Fuller, Geoff Vasil, Kyle Augustson, Matteo Cantiello, Stephane Mathis, and Conny Aerts for useful discussions regarding IGWs, magnetic fields, and dynamo physics. DL is supported in part by NASA HTMS grant 80NSSC20K1280. DMB and TVR gratefully acknowledge funding from the Research Foundation Flanders (FWO) by means of senior and junior postdoctoral fellowships with grant agreements 1286521N and 12ZB620N, respectively, and FWO long stay travel grants V411621N and V414021N, respectively. Computations were conducted with support by the NASA High End Computing (HEC) Program through the NASA Advanced Supercomputing (NAS) Division at Ames Research Center on Pleiades with allocation GIDs s2276. The authors are grateful to the staff and scientists at the Kavli Institute for Theoretical Physics, University of California, Santa Barbara, and to the (other) organisers of the ‘Probes of Transport in Stars’ program, which hosted them during this work. This research was supported in part by the National Science Foundation under Grant No. NSF PHY-1748958.

DATA AVAILABILITY

All generated data and scripts used to make the figures for this paper are provided at <https://github.com/lecoanet/HD43317-B>.

REFERENCES

Aerts C., 2021, *Reviews of Modern Physics*, **93**, 015001
Aerts C., Christensen-Dalsgaard J., Kurtz D. W., 2010, *Asteroseismology*. Springer
Augustson K. C., Brun A. S., Toomre J., 2016, *ApJ*, **829**, 92
Auvergne M., et al., 2009, *A&A*, **506**, 411
Bouabid M.-P., Dupret M.-A., Salmon S., Montalbán J., Miglio A., Noels A., 2013, *MNRAS*, **429**, 2500
Bowman D. M., 2020, *Frontiers in Astronomy and Space Sciences*, **7**, 70
Briquet M., Neiner C., Leroy B., Pápics P. I., MiMeS Collaboration 2013, *A&A*, **557**, L16
Burns K. J., Vasil G. M., Oishi J. S., Lecoanet D., Brown B. P., 2020, *Physical Review Research*, **2**, 023068

Buysschaert B., Neiner C., Briquet M., Aerts C., 2017, *A&A*, **605**, A104
Buysschaert B., Aerts C., Bowman D. M., Johnston C., Van Reeth T., Pedersen M. G., Mathis S., Neiner C., 2018, *A&A*, **616**, A148
Cantiello M., Fuller J., Bildsten L., 2016, *ApJ*, **824**, 14
Featherstone N. A., Browning M. K., Brun A. S., Toomre J., 2009, *ApJ*, **705**, 1000
Fuller J., Cantiello M., Stello D., García R. A., Bildsten L., 2015, *Science*, **350**, 423
García R. A., et al., 2014, *A&A*, **563**, A84
Goldstein J., Townsend R. H. D., 2020, *ApJ*, **899**, 116
Grunhut J. H., et al., 2017, *MNRAS*, **465**, 2432
Johnston C., 2021, *A&A*, **655**, A29
Keszthelyi Z., Meynet G., Georgy C., Wade G. A., Petit V., David-Uraz A., 2019, *MNRAS*, **485**, 5843
Lecoanet D., Vasil G. M., Fuller J., Cantiello M., Burns K. J., 2017, *MNRAS*, **466**, 2181
Lecoanet D., Vasil G. M., Burns K. J., Brown B. P., Oishi J. S., 2019, *Journal of Computational Physics: X*, p. 100012
Maeder A., Meynet G., 2005, *A&A*, **440**, 1041
Mestel L., 1999, *Stellar magnetism*. International series of monographs on physics Vol. 99, Oxford
Miglio A., Montalbán J., Noels A., Eggenberger P., 2008, *MNRAS*, **386**, 1487
Mombarg J. S. G., Van Reeth T., Pedersen M. G., Molenberghs G., Bowman D. M., Johnston C., Tkachenko A., Aerts C., 2019, *MNRAS*, **485**, 3248
Neiner C., Mathis S., Alecian E., Emeriau C., Grunhut J., BinaMiCS MiMeS Collaborations 2015, in Nagendra K. N., Bagnulo S., Centeno R., Jesús Martínez González M., eds, *IAU Symposium Vol. 305, Polarimetry*. pp 61–66 ([arXiv:1502.00226](https://arxiv.org/abs/1502.00226)), doi:10.1017/S1743921315004524
Pápics P. I., et al., 2012, *A&A*, **542**, A55
Pápics P. I., et al., 2017, *A&A*, **598**, A74
Paxton B., Bildsten L., Dotter A., Herwig F., Lesaffre P., Timmes F., 2011, *ApJS*, **192**, 3
Paxton B., et al., 2013, *ApJS*, **208**, 4
Paxton B., et al., 2015, *ApJS*, **220**, 15
Pedersen M. G., et al., 2021, *Nature Astronomy*, **5**, 715
Power J., 2007, Master’s thesis, Queen’s University, Canada
Prat V., Mathis S., Buysschaert B., Van Beeck J., Bowman D. M., Aerts C., Neiner C., 2019, *A&A*, **627**, A64
Prat V., Mathis S., Neiner C., Van Beeck J., Bowman D. M., Aerts C., 2020, *A&A*, **636**, A100
Ricker G. R., et al., 2015, *Journal of Astronomical Telescopes, Instruments, and Systems*, **1**, 014003
Schneider F. R. N., Ohlmann S. T., Podsiadlowski P., Röppe F. K., Balbus S. A., Pakmor R., Springel V., 2019, *Nature*, **574**, 211
Shultz M., Wade G. A., Grunhut J., Hanes D., Bagnulo S., Landstreet J. D., MiMeS Collaboration 2012, in Drissen L., Robert C., St-Louis N., Moffat A. F. J., eds, *Astronomical Society of the Pacific Conference Series Vol. 465, Proceedings of a Scientific Meeting in Honor of Anthony F. J. Moffat*. p. 101
Shultz M. E., et al., 2018, *MNRAS*, **475**, 5144
Stello D., Cantiello M., Fuller J., Huber D., García R. A., Bedding T. R., Bildsten L., Silva Aguirre V., 2016, *Nature*, **529**, 364
Townsend R. H. D., Teitler S. A., 2013, *MNRAS*, **435**, 3406
Townsend R. H. D., Goldstein J., Zweibel E. G., 2018, *MNRAS*, **475**, 879
Van Beeck J., Prat V., Van Reeth T., Mathis S., Bowman D. M., Neiner C., Aerts C., 2020, *A&A*, **638**, A149
Van Reeth T., Tkachenko A., Aerts C., 2016, *A&A*, **593**, A120
Vasil G. M., Lecoanet D., Burns K. J., Oishi J. S., Brown B. P., 2019, *Journal of Computational Physics: X*, p. 100013
Wade G. A., et al., 2014, in Petit P., Jardine M., Spruit H. C., eds, *IAU Symposium Vol. 302, Magnetic Fields throughout Stellar Evolution*. pp 265–269 ([arXiv:1310.3965](https://arxiv.org/abs/1310.3965)), doi:10.1017/S1743921314002233
Wade G. A., et al., 2016, *MNRAS*, **456**, 2

This paper has been typeset from a \LaTeX file prepared by the author.